Atmospheric
Chemistry
and Physics

Open Access

Constraints on Asian ozone using Aura TES, OMI and Terra MOPITT

Z. Jiang[1], J. R. Worden[1], D. B. A. Jones[2,3], J.-T. Lin[4], W. W. Verstraeten[5,6], and D. K. Henze[7]

[1]Jet Propulsion Laboratory, California Institute of Technology, Pasadena, CA, USA
[2]Department of Physics, University of Toronto, Toronto, ON, Canada
[3]JIFRESSE, University of California, Los Angeles, Los Angeles, CA, USA
[4]Laboratory for Climate and Ocean-Atmosphere Studies, Department of Atmospheric and Oceanic Sciences, School of Physics, Peking University, Beijing, China
[5]Meteorology and Air Quality Department, Wageningen University, the Netherlands
[6]Climate Observations Department, Royal Netherlands Meteorological Institute, the Netherlands
[7]Department of Mechanical Engineering, University of Colorado, Boulder, CO, USA

Correspondence to: Z. Jiang (zhe.jiang@jpl.nasa.gov)

Abstract. Rapid industrialization in Asia in the last two decades has resulted in a significant increase in Asian ozone (O_3) precursor emissions with likely a corresponding increase in the export of O_3 and its precursors. However, the relationship between this increasing O_3, the chemical environment, O_3 production efficiency, and the partitioning between anthropogenic and natural precursors is unclear. In this work, we use satellite measurements of O_3, CO and NO_2 from TES (Tropospheric Emission Spectrometer), MOPITT (Measurement of Pollution In The Troposphere) and OMI (Ozone Monitoring Instrument) to quantify O_3 precursor emissions for 2006 and their impact on free tropospheric O_3 over northeastern Asia, where pollution is typically exported globally due to strong westerlies. Using the GEOS-Chem (Goddard Earth Observing System Chemistry) global chemical transport model, we test the modeled seasonal and interannual variation of O_3 based on prior and updated O_3 precursor emissions where the updated emissions of CO and NO_x are based on satellite measurements of CO and NO_2. We show that the observed TES O_3 variability and amount are consistent with the model for these updated emissions. However, there is little difference in the modeled ozone between the updated and prior emissions. For example, for the 2006 June time period, the prior and posterior NO_x emissions were 14 % different over China but the modeled ozone in the free troposphere was only 2.5 % different. Using the adjoint of GEOS-Chem we partition the relative contributions of natural and anthropogenic sources to free troposphere O_3 in this region. We find that the influence of lightning NO_x in the summer is comparable to the contribution from surface emissions but smaller for other seasons. China is the primary contributor of anthropogenic CO, emissions and their export during the summer. While the posterior CO emissions improved the comparison between model and TES by 32 %, on average, this change also had only a small effect on the free tropospheric ozone. Our results show that the influence of India and southeastern Asia emissions on O_3 pollution export to the northwestern Pacific is sizeable, comparable with Chinese emissions in winter, about 50 % of Chinese emissions in spring and fall, and approximately 20 % of the emissions in the summer.

1 Introduction

Unprecedented growth in transportation, coal-fired power plants and the industrial sector in China has resulted in a substantial increase in the emissions of O_3 precursors (Lin et al., 2014a). Recent studies (Lamsal et al., 2011; Lin, 2012; Mijling et al., 2013) show a 5–10 % annual growth rate of NO_x emission in China. Wang et al. (2012) found there was a 3 % annual growth rate of O_3 in Beijing in the period of

2003–2010. East Asian O_3 can be transported to the surface of North America in about 2–3 weeks (Liu and Mauzerall, 2005) by midlatitude westerly winds (Liang et al., 2004, 2005), which likely resulted in an increase of background O_3 concentration in western North America by 3–7 ppbv (parts per billion by volume) during the period of 2000–2006 (Zhang et al., 2008; Brown et al., 2011).

Use of inverse (top-down) methods to better quantify the emission of NO_x (Lamsal et al., 2011; Lin and McElroy, 2011; Lin, 2012; Mijling et al., 2013), VOCs (volatile organic compounds; Shim et al., 2005; Fu et al., 2007) and CO (Kopacz et al., 2010; Fortems-Cheiney et al., 2011; Gonzi et al., 2011) are needed to ensure consistency between bottom-up inventories and observations. However, large discrepancies can still exist between bottom-up- and top-down-based inventories (e.g., Kopacz et al., 2010; Lin et al., 2012). In this work, we perform a multi-tracer assimilation with the GEOS-Chem (Goddard Earth Observing System Chemistry) model to evaluate the top-down estimates of O_3 precursors (NO_x and CO) in eastern Asia. We firstly optimized the CO and NO_x emission with MOPITT (Measurements Of Pollution In The Troposphere) CO and OMI (Ozone Monitoring Instrument) NO_2 retrievals, respectively, and then evaluate the a posteriori simulation of CO and O_3 by comparing the values with measurements from TES (Tropospheric Emission Spectrometer) in the period of December 2005–November 2006. Using the adjoint of the GEOS-Chem model (Henze et al., 2007), we then quantify source contributions (NO_x, CO, VOC) to free tropospheric O_3 pollution over eastern China and the China outflow region in December 2005–November 2006.

2 Observations and model

2.1 TES CO and O_3

The TES instrument was launched on NASA's Aura spacecraft on 15 July 2004. The satellite is in a sun-synchronous polar orbit of 705 km and crosses the Equator at 01:45 and 13:45 LT (local time). With a footprint of 8 km × 5 km, TES measures radiances between 3.3 and 15.4 μm with a global coverage in 16 days (Beer et al., 2001) of observations. In the troposphere, TES O_3 profile retrievals have 1–2 degrees of freedom for signal (DOFS), and about 1 DOFS for CO. We use data from the "lite" product (http://tes.jpl.nasa.gov/data/) which reports volume mixing ratios (VMRs) on 26 pressure levels for O_3 and 14 pressure levels for CO. Using an optimal estimation approach, the TES retrievals are conducted with respect to the logarithm of the VMR. The relationship between the retrieved profiles and the true atmospheric state can be expressed as

$$\hat{z}^{TES} = z_a^{TES} + A^{TES}(z - z_a^{TES}) + G\varepsilon, \qquad (1)$$

where z is the true atmospheric state (expressed as log(VMR)), z_a^{TES} is the TES a priori O_3 or CO profile, A^{TES} is the TES averaging kernel matrix and $G\varepsilon$ describes the retrieval error. The averaging kernel matrix represents the sensitivity of the retrieval to the actual trace gas in the atmosphere. The TES retrievals use a monthly mean profile of the trace gas from the MOZART-4 CTM (chemical transport model), averaged over a 10° latitude × 60° longitude, as the a priori information z_a^{TES}. According to the recommended quality control criterion, we only use CO and O_3 data with major quality flags of 1. These data have passed all major quality flags used to assess the TES data related to chi-2 tests, biases in the radiance residuals, and residual nonlinearity checks. The data with small DOFS (DOFS for CO smaller than 0.8) are dropped as the limited sensitivity reduces the robustness of calculated O_3–CO correlations. We empirically find that the sensitivity of CO is the limiting factor in these comparisons; that is, if DOFS for CO is > 0.8 then the DOFS of O_3 is > 0.8. Recently, Verstraeten et al. (2013) evaluated TES O_3 measurements by using data from the World Ozone and Ultraviolet Radiation Data Centre (WOUDC) sites and found that there is a ∼ 7 ppb bias in the TES measurements in free troposphere, and that the magnitude is slightly larger in summer and smaller in winter. TES CO measurements were evaluated by Luo et al. (2007) using the aircraft measurements from INTEX-B (Intercontinental Chemical Transport Experiment B) campaign. They showed that TES CO VMR profiles are 0–10 % lower than the aircraft measurements in the lower and middle troposphere.

2.2 MOPITT CO

The MOPITT instrument was launched on NASA's Terra spacecraft on 18 December 1999. The satellite is in a sun-synchronous polar orbit of 705 km and crosses the Equator at 10:30 LT. With a footprint of 22 km × 22 km, MOPITT (version 6) combines TIR (thermal infrared; 4.7 μm) with the NIR (near infrared; 2.3 μm) and has better sensitivity to lower tropospheric CO over land (Worden et al., 2010). MOPITT CO retrievals are reported on 10 pressure levels (surface, 900, 800, 700, 600, 500, 400, 300, 200 and 100 hPa). Similar to the TES product, relationship between the retrieved CO profiles and the true atmospheric state can be expressed as

$$z^{MOP} = z_a^{MOP} + A^{MOP}(z - z_a^{MOP}) + G\varepsilon, \qquad (2)$$

where z is the true atmospheric state (expressed as log(VMR)), z_a^{MOP} is the MOPITT a priori CO profile, A^{MOP} is the MOPITT averaging kernel matrix and $G\varepsilon$ describes the retrieval error.

Same as TES, the a priori information of MOPITT retrievals is from the monthly mean profile of the MOZART-4 CTM, without the 10° latitude × 60° longitude average. We reject MOPITT data with CO column amounts of less than 5×10^{17} molec cm^{-2} and if low clouds are observed. The nighttime data are excluded in the assimilation, due to

the NIR radiances measured reflected solar radiation. The version 5 data have been evaluated recently against NOAA aircraft measurements (Deeter et al., 2013), which shows a small bias in the low and middle troposphere, but 14 % positive bias at the 200 hPa retrieval level. The new version 6 data significantly reduce the bias in the upper troposphere but magnify the positive bias at the surface level. In this work, we decide to use the new version 6 data, as we focus on the free troposphere (above 800 hPa), which is not affected by the positive bias in the retrieval at the surface level.

2.3 OMI NO$_2$

The OMI instrument was also launched on NASA's Aura spacecraft. The sensor has a spatial resolution of 13 km × 24 km (Levelt et al., 2006). OMI provides daily global coverage with measurements of both direct and atmosphere-backscattered sunlight in the ultraviolet–visible range from 270 to 500 nm; 405–465 nm is used to retrieve tropospheric NO$_2$ columns. In this study, the daily level-2 data from the KNMI (Royal Netherlands Meteorological Institute) DOMINO-2 product (Derivation of OMI tropospheric NO2; Boersma et al., 2011) are averaged to obtain monthly mean vertical column densities (VCDs) for subsequent emission inversion. The total error for the retrieved VCDs is about 30 % plus 0.7×10^{15} molec cm^{-2}, and the magnitude is larger in winter than in summer (Boersma et al., 2011; Lin and McElroy, 2011). The pixels with cloud radiance fraction exceeding 50 % are removed. In order to have a better analysis of the spatial distribution of VCDs within short distance, we only use data from the 30 pixels around the swath center. The details for the data treatment are described in Lin (2012).

2.4 GEOS-Chem

The GEOS-Chem CTM (http://www.geos-chem.org) is driven by assimilated meteorological observation from the NASA Goddard Earth Observing System (GEOS-5) at the Global Modeling and data Assimilation Office. We use version v34 of the GEOS-Chem adjoint, which is based on v8-02-01 of GEOS-Chem, with relevant updates through v9-01-01. The standard GEOS-Chem chemistry mechanism includes 43 tracers, which can simulate detailed tropospheric O$_3$–NO$_x$–hydrocarbon chemistry, including the radiative and heterogeneous effects of aerosols. The GEOS-5 meteorological fields have 72 vertical levels and the lowest 31 levels are terrain following levels. In order to minimize the amount of memory required to run GEOS-Chem, the model is run with a reduced vertical resolution, in which the levels in the stratosphere are lumped together online.

The native horizontal resolution of GEOS-5 is 0.5° × 0.667°, but it is usually degraded to 4° × 5° or 2° × 2.5° in global-scale simulations. A nested simulation can be achieved by running a 0.5° × 0.667° resolution model

within a regional domain using the boundary condition provided from a global, coarse-resolution mode (Wang et al., 2004; Chen et al., 2009). Recently, the adjoint of nested GEOS-Chem was developed by Jiang et al. (2014a). In this work, following Jiang et al. (2014a) and Mao et al. (2014), we run the model with 0.5° × 0.667° resolution over Asia. The boundary condition is generated with a global-scale 4° × 5°-resolution simulation.

The anthropogenic emission inventories are identical to those used in Jiang et al. (2013). The global anthropogenic emission inventory is EDGAR (Emission Database for Global Atmospheric Research) version 3.2FT2000 (Olivier et al., 2001), updated by the following regional emission inventories: the INTEX-B Asia emissions inventory for 2006 (Q. Zhang et al., 2009), the Cooperative program for monitoring and evaluation of the long-range transmission of air pollutants in Europe (EMEP) inventory for Europe in 2000 (Vestreng et al., 2002), the US Environmental Protection Agency National Emission Inventory (NEI) for 2005 in North America, the Criteria Air Contaminants (CAC) inventory for Canada, and the Big Bend Regional Aerosol and Visibility Observational (BRAVO) Study Emissions Inventory for Mexico (Kuhns et al., 2003). Biomass burning emissions are from the interannual GFED3 (Global Fire Emissions Database) inventory with 3 h resolution (van der Werf et al., 2010). The biogenic emissions are from MEGAN 2.0 (Model of Emissions of Gases and Aerosols from Nature version 2; Millet et al., 2008). Figure 1 shows the anthropogenic emission of NO$_x$ and CO in Asia in June 2006. There are strong pollutant emissions in the North China Plain. The urban emission centers can also be clearly identified. The annual anthropogenic NO$_x$ emission over eastern China is 16.5 Tg (2006) and 20.7 Tg (2010), with a 5 % annual growth rate.

3 Inversion approach

3.1 4-DVAR inversion for global CO emission

In this work, we evaluate the observed interannual variability of O$_3$ and CO and the GEOS-Chem model simulation for the period of 2006–2010, where the data density of TES measurements is higher relative to subsequent years. As the first year of this 5-year period, the relative contributions of O$_3$ precursors to free troposphere O$_3$ in 2006 will be studied in detail. The 2006 global CO emissions are optimized with a 4-DVAR (four-dimensional variational) method. The inverse method minimizes the cost function $J(x)$ to provide an optimal estimate of the CO sources,

$$J(x) = (F(x) - y)^T \mathbf{S}_\Sigma^{-1} (F(x) - y) + (x - x_a)^T$$
$$\mathbf{S}_a^{-1} (x - x_a), \tag{3}$$

where x is the state vector of emissions, x_a is the a priori estimate, y is a vector of observed concentrations, and $F(x)$

is the forward model, which represents the transport of the CO emissions in the GEOS-Chem model and accounts for the vertical smoothing of the MOPITT retrieval. S_Σ and S_a are the observational and a priori error covariance matrices, respectively. The first term of the cost function represents the mismatch between the simulated and observed concentrations. The second term represents the departure of the estimate from the a priori.

The cost function in Eq. (3) is minimized by reducing the gradient, $\partial J / \partial x$, using the adjoint of GEOS-Chem model in a 4-DVAR approach (Henze et al., 2007), which has been previously used for assimilation of CO and O_3 (Kopacz et al., 2010; Singh et al., 2011; Parrington et al., 2012; Jiang et al., 2014b). Similar to Jiang et al. (2013, 2014b), we produce improved initial conditions by assimilating MOPITT version 6 data, using the sequential sub-optimal Kalman filter (Parrington et al., 2008), from 1 January 2006 to 1 January 2007. The optimized initial conditions are archived at the beginning of each month. Consequently, the initial conditions for the model simulation are independent from the inverse analyses.

3.2 Regression-based inversion for China NO_x emissions

The 2006 Chinese NO_x emissions are optimized with a regression-based multistep method exploiting the distinctive seasonality of different sources (Lin, 2012). Neglecting horizontal transport and assuming a linear relationship between the total VCD of NO_2 and VCDs from individual sources, the predicted VCD (Ω_p) for a given grid can be expressed as the sum of individual emission sources, multiplied by certain scaling factors:

$$\Omega_p = k_a\Omega_a + k_l\Omega_l + k_s\Omega_s + k_b\Omega_b. \tag{4}$$

The subscripts "a", "l", "s", and "b" indicate anthropogenic, lightning, soil and biomass burning sources of NO_x, respectively. The updated emission estimates can be obtained by reducing the sum of $[(\Omega_r - \Omega_p)/\sigma]^2$ across the 12 months; here Ω_r is the retrieved VCD and σ is the standard deviation. To better represent the resolution-dependent NO_x chemistry (Valin et al., 2011), the inversion was conducted with the highest resolution of GEOS-Chem. The seasonality-based inversion method also reduced the influence of potential biases in OMI NO_2 data (Lin et al., 2014b), particularly in winter. The details for the inversion process were described in Lin (2012).

4 Results and discussion

4.1 Evaluation of the model simulation and top-down estimates of O_3 precursors

In this work, we are interested in the domain of eastern China, as shown in Fig. 1, because it is the largest pollu-

tant emission contributor in eastern Asia and the adjacent domain where outflow of Asian pollution is significant. Figure 2 shows the monthly regional mean O_3 and CO concentration at the free troposphere (681–383 hPa) for June, July and August for the period 2006–2010, using the GEOS-Chem model driven with a priori emission inventories. The modeled O_3 concentrations are generally within 10 % of the TES data after accounting for the approximately 7 ppb bias in the TES O_3 measurements (e.g., Worden et al., 2007; Verstraeten et al., 2013). However, the modeled CO is biased low, which is consistent with previous studies (Shindell et al., 2006; Kopacz et al., 2010; Naik et al., 2013). This low bias could be associated with a positive bias in OH, as indicated by Jiang et al. (2014b). The bias in CO can be reduced by integrating the coarse-resolution global and fine-resolution nested simulations in a two-way coupled manner, such that results from the nested model can be used to improve the global model (within the nested domain) and ultimately affect its lateral boundary conditions (via the global transport of CO and other species) (Yan et al., 2014). Another possible reason for the CO bias is that the TES CO data are biased towards polluted air parcels because of its relatively low sensitivity whereas the model captures background values as discussed in Pechony et al. (2013). Although the model is biased low, the interannual variabilities and trends of O_3 and CO are well correlated between the model and TES, indicating that changes in the modeled emissions, chemical production of ozone, and meteorology are well described (e.g., Zhang et al., 2006; Kim et al., 2013).

O_3–CO correlations can be used to constrain O_3 sources and transport (e.g., Zhang et al., 2006). Positive correlations usually indicate that a region has experienced photochemical O_3 production, whereas negative correlations may result from O_3 chemical loss or influence of stratospheric air. For example, Zhang et al. (2006) demonstrated that TES data can be used to examine global distribution of O_3–CO correlations. Voulgarakis et al. (2011) found significant positive correlations in the northern Pacific during the summer of 2005–2008. Kim et al. (2013) used OMI O_3 and AIRS (Atmospheric Infrared Sounder) CO to show that the GEOS-Chem model is able to reproduce the observed O_3-CO correlations and slopes in the western Pacific, but failed in some tropical regions due to model transport error associated with deep convection.

Table 1 shows the monthly regional mean O_3 and CO correlation and slope values for the free troposphere (825–383 hPa) for June, July and August 2006–2010; the model is driven by a priori emissions. The uncertainty in the O_3 and CO concentrations are due to random errors in the TES O_3 and CO observations and natural variability (Zhang et al., 2006). For this reason, we also show the mean value over the analysis time period. The correlation and slope values of TES and GEOS-Chem are generally consistent for both domains. The positive correlation coefficients imply influence of photochemical O_3 production but also transport of nearby CO
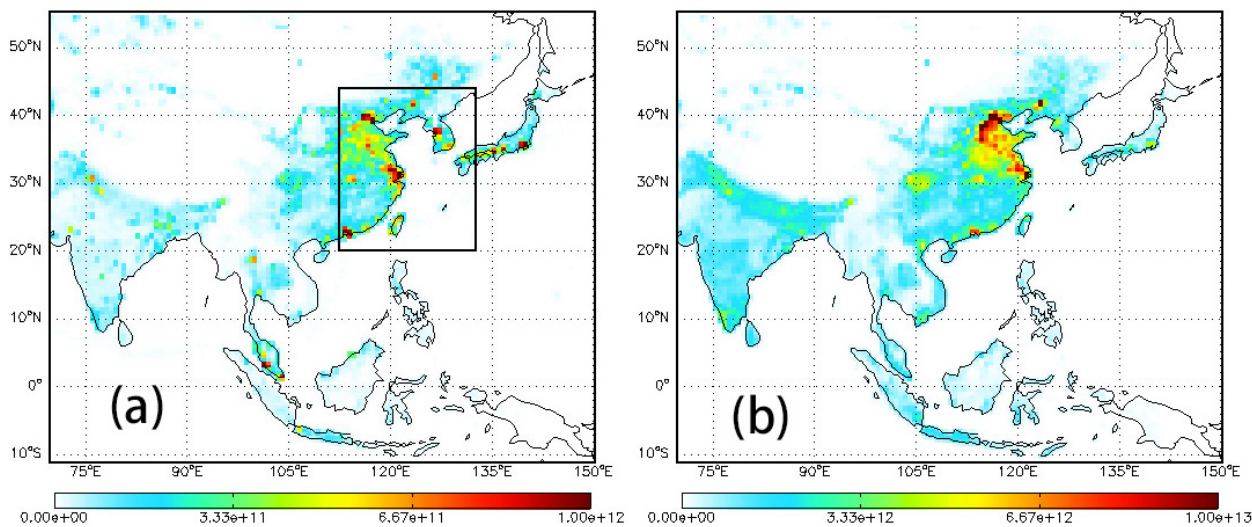
Figure 1. Anthropogenic emission of (a) NO$_x$ and (b) CO in June 2006 as used in GEOS-Chem. The unit is in molecules per square centimeter per second (molec cm^{-2} s^{-1}). The black box defines the domains studied in this work. The "eastern China" domain includes the grids of Chinese mainland within the black box. The "China outflow region" are grids within the black box, excluding the Chinese mainland.
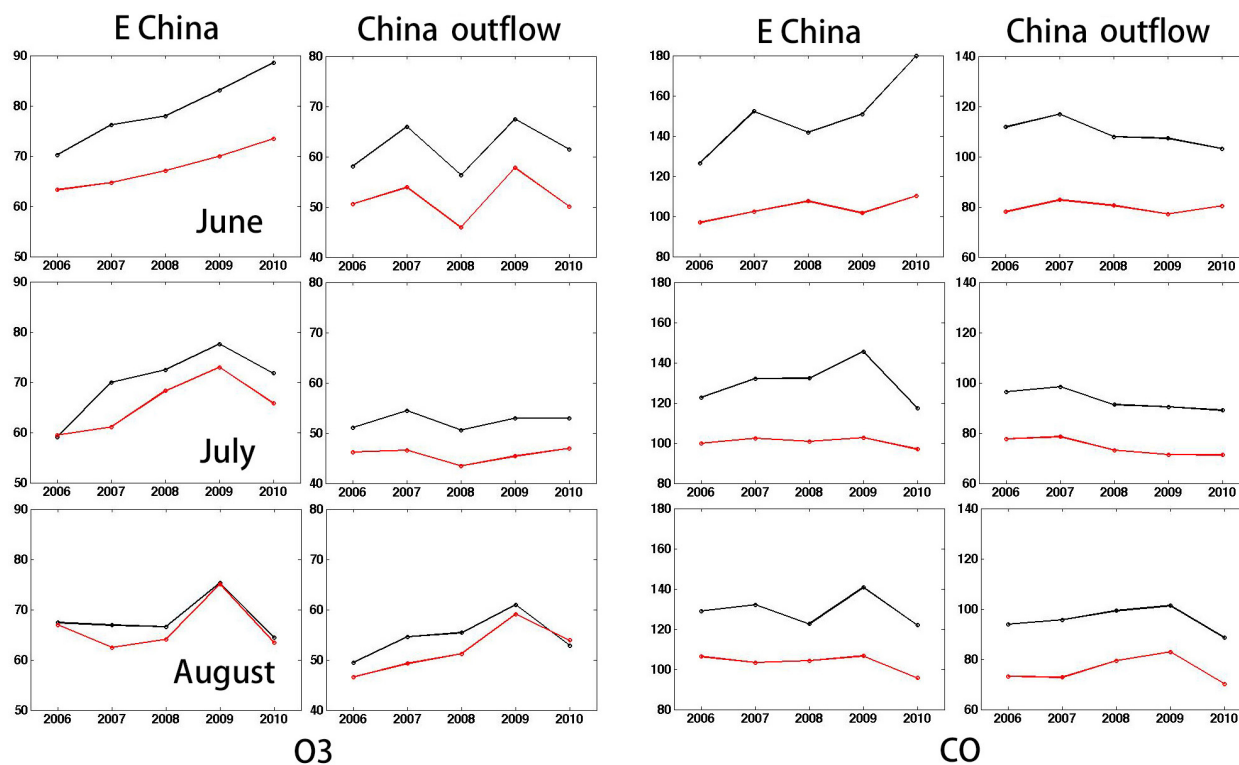
Figure 2. Monthly regional mean O$_3$ and CO concentration at free troposphere (681–383 hPa) in June, July and August 2006–2010. The red line is the GEOS-Chem model simulation with a priori emission inventories and the black line represents the TES measurements. The model results are smoothed with the TES averaging kernels. The TES ozone data are biased high by 7 ppbv.

emissions into pollution plumes (e.g., Worden et al., 2013) As in previous studies (Zhang et al., 2006; Voulgarakis et al., 2011; Kim et al., 2013), there are small differences between the simulation and observation. A possible reason for these discrepancies, particularly over the ocean, is the model transport error because transport of "clean" air from the Pacific can have substantially different chemical characteristics to Asian air.

Table 1. Monthly regional mean O_3 and CO correlation and slope for the free troposphere (825–383 hPa) for June, July and August 2006–2010 for both TES and model (in parentheses). The model values are sampled at the TES measurement time and location and smoothed with the TES averaging kernels. The calculation of slope and correlation is based on individual measurements within a month. The numbers of measurements used to compute the correlations are shown in the Supplement. The far-right column is the mean value of 15 months.

Region	Type	Month	2006	2007	2008	2009	2010	Mean
Eastern China	dO_3/dCO	Jun	0.36 (0.25)	0.17 (−0.06)	0.19 (0.14)	0.14 (0.02)	0.18 (0.29)	
		Jul	0.08 (0.38)	0.29 (0.36)	0.23 (0.34)	0.15 (0.44)	0.38 (0.19)	0.22 (0.25)
		Aug	0.20 (0.27)	0.22 (0.26)	0.32 (0.20)	0.15 (0.18)	0.29 (0.47)	
	R	Jun	0.66 (0.39)	0.47 (−0.11)	0.45 (0.30)	0.51 (0.10)	0.70 (0.52)	
		Jul	0.23 (0.61)	0.66 (0.57)	0.49 (0.38)	0.50 (0.57)	0.53 (0.24)	0.50 (0.37)
		Aug	0.33 (0.38)	0.52 (0.43)	0.54 (0.28)	0.39 (0.22)	0.56 (0.64)	
China outflow	dO_3/dCO	Jun	0.32 (0.60)	0.49 (0.43)	0.52 (0.62)	0.59 (0.66)	0.64 (0.76)	
		Jul	0.56 (0.59)	0.50 (0.48)	0.65 (0.83)	0.63 (1.05)	0.75 (1.13)	0.55 (0.70)
		Aug	0.55 (0.85)	0.32 (0.49)	0.51 (0.61)	0.53 (0.51)	0.67 (0.89)	
	R	Jun	0.69 (0.57)	0.71 (0.41)	0.76 (0.62)	0.68 (0.35)	0.73 (0.55)	
		Jul	0.73 (0.57)	0.66 (0.47)	0.66 (0.69)	0.59 (0.70)	0.73 (0.78)	0.67 (0.57)
		Aug	0.68 (0.71)	0.55 (0.46)	0.63 (0.60)	0.58 (0.39)	0.74 (0.75)	

The consistency between the model and TES in the interannual variations, correlation coefficients and slopes implies that the spatiotemporal distribution of the CO emissions and oxidative chemical processes are consistent. As described in Sect. 3, the 2006 global CO emissions are constrained with MOPITT data; the 2006 Chinese NO_x emission are constrained with OMI data. As shown in Fig. 3, Chinese posterior anthropogenic NO_x emissions in June 2006 increased by 14 % over the a priori emissions, from 1.86 to 2.11 Tg. Smaller adjustments are obtained for winter. In June 2006, the Chinese anthropogenic CO emissions increased from 17.09 to 18.93 Tg, with a mean scaling factor of 1.11. In December 2005, the Chinese *posterior* anthropogenic CO emission increased over the prior from 14.95 to 19.78 Tg. However, as indicated by Jiang et al. (2014b), a potential bias in OH fields could have a significant influence on the inferred CO emission estimates. By using the OH fields from a different GEOS-Chem version, they found that a posteriori CO emissions over eastern Asia in June–August 2004 are reduced by 28 % for the different OH fields. This large potential error in the CO emissions do not strongly affect our conclusions because the modeled CO concentrations, based on the model OH distributions and CO emissions, are consistent with the MOPITT data.
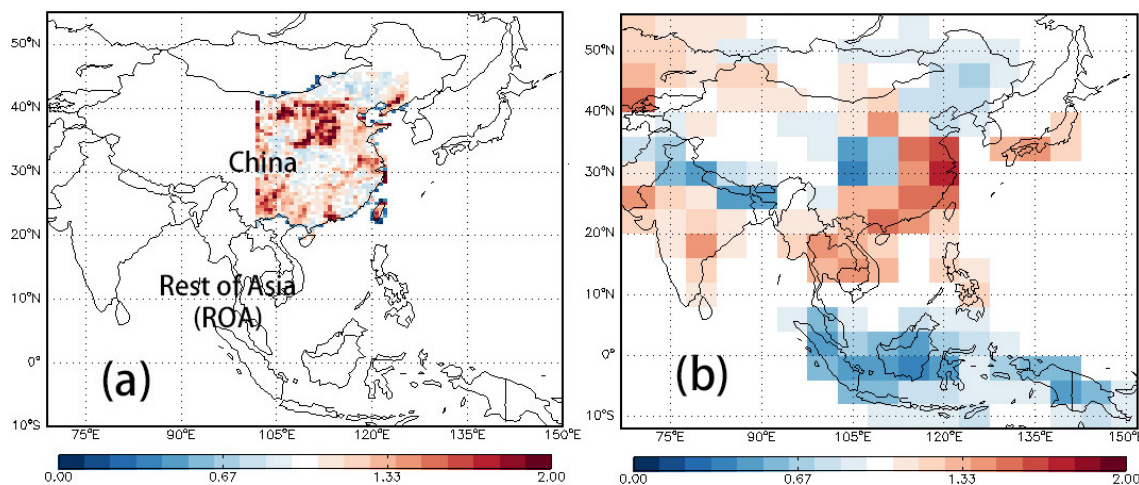
The monthly regional mean O_3 and CO concentrations in the period of December 2005–November 2006 are shown in Fig. 4. In order to remove the influence of the initial conditions, the updated simulation is obtained by running the model from 1 September 2005, with updated inventories of NO_x and CO. Both the model and data show increases of O_3 concentration from winter to spring, due to enhancement of photochemical production, and a substantial decrease in June–August, due to the effect of the East Asian monsoon (Yang et al., 2014). The CO concentration peaks in March,

which is consistent with Shindell et al. (2006). The boreal spring CO maximum is associated with the accumulation of CO emissions in winter, while CO lifetime is longer (Duncan et al., 2007). The updated inventories significantly reduced the bias on the CO simulation. However, these changes in the NO_x and CO emissions do not significantly change free tropospheric ozone.

4.2 Dependency of O_3 on anthropogenic and natural NO_x, CO and VOCs

In this section, we will use the adjoint of the GEOS-Chem model (Henze et al., 2007) to quantify source contributions (NO_x, CO, VOC) to free tropospheric O_3 pollution over eastern China and the China outflow region. The updated NO_x and CO emission inventories are intended to improve the simulation. We are interested in these two domains as they have significant influence on the long-range pollution transport (e.g., L. Zhang et al., 2009). Similar to previous studies (L. Zhang et al., 2009; Bowman and Henze, 2012; Lapina et al., 2014), the analysis is based on a sensitivity calculation from an adjoint model. In this work, both transport and chemistry components are run backwards and thus provide a more computationally efficient method for a receptor-oriented problem than the traditional approach by perturbing emissions.

Figure 5 shows the contributions of anthropogenic NO_x, lightning NO_x, anthropogenic CO and biogenic isoprene on free tropospheric (819–396 hPa) O_3 over eastern China. The value can be explained as the percentage change of regional mean O_3 due to a fractional change in emissions in a particular grid. For example, assuming an unchanged chemical environment, one particular grid with contribution 0.02 % implies mean free tropospheric O_3 over eastern China will

Figure 3. (a) Scaling factors of anthropogenic NO_x for June 2006. **(b)** Scaling factor of total CO emission (combustion + oxidation from biogenic VOCs) for June 2006.
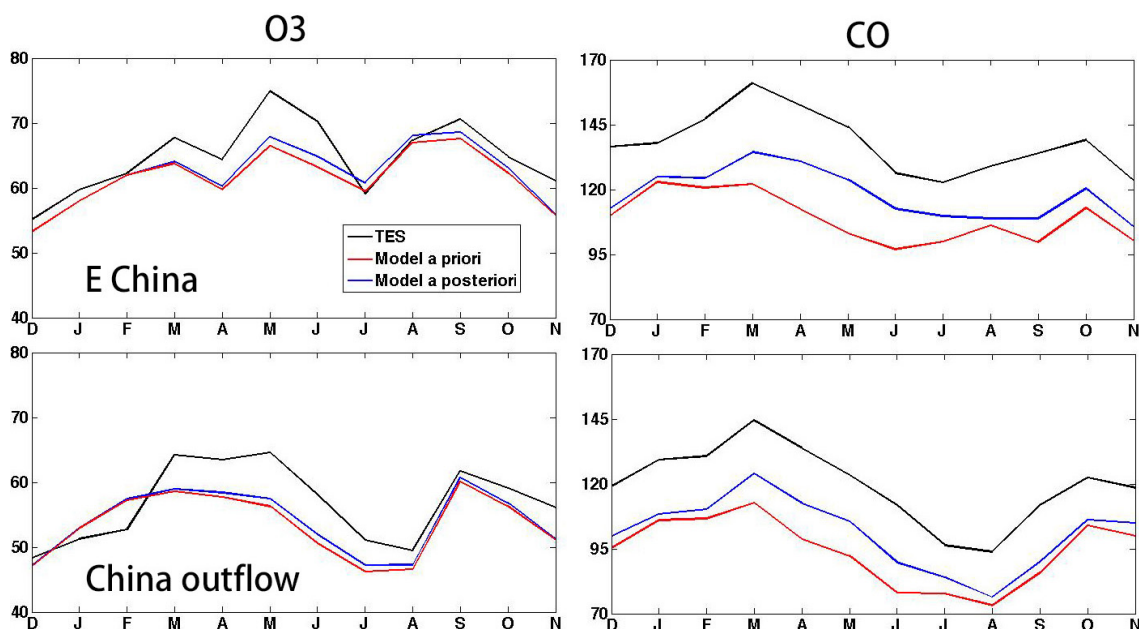
Figure 4. Monthly regional mean O_3 and CO concentration at free troposphere (681–383 hPa) in the period of December 2005–November 2006. The red line is GEOS-Chem model simulation with a priori emission inventories. The blue line is model simulation with updated NO_x and CO emission inventories. The black line represents TES measurements. The model results are smoothed with the TES averaging kernels. The positive bias in the TES O_3 data is larger in summer and smaller in winter.

be increased by 0.02 %, if the NO_x emission in this gird is increased by 100 %. The result shows that anthropogenic NO_x contributes significantly to the O_3 distribution in this region. Although the influence of lightning NO_x is weaker, the larger geographical distribution of lightning NO_x makes it an important source. The contribution of anthropogenic CO is mainly from China, whereas southeastern Asia is the major contributor of biogenic isoprene with a negative sensitivity. Assuming anthropogenic CO is a proxy of anthropogenic hydrocarbons and biogenic isoprene is a proxy of

biogenic hydrocarbons, these sensitivity calculations indicate that China is a major source of anthropogenic hydrocarbons while southeastern Asia is the major source of biogenic hydrocarbons. As shown in Fig. 1, the North China Plain has strong NO_x emissions, but their effect on O_3 is not significant. However, eastern China free tropospheric O_3 is more directly sensitive to CO emissions from the North China Plain. The contribution of CO to ozone production (third set of panels in Fig. 5) is similar to the CO emissions distribution. Discrepancies exist between the spatial distribution of

the sensitivity of ozone to NO_x and CO. For example, the sensitivity of ozone to NO_x in the Beijing area is relatively small because there is too much NO_x, thus limiting ozone production. Martin et al. (2004) showed that an increase of NO_x emission over northeastern China in summer will decrease surface O_3 concentration, which is opposite to the positive sensitivity in this work. This difference could be associated with the larger concentrations of VOC levels (e.g., Zhang et al., 2014) and because the sensitivities shown in Fig. 5 depend on both surface ozone production and ozone production in the free troposphere, which is more NO_x limited.

It should be reminded that the sensitivity of ozone to biogenic isoprene is highly dependent on the isoprene chemistry scheme, as indicated by Mao et al. (2013). They demonstrated that the sensitivity of surface O_3 concentration over the southeastern United States on isoprene could change sign, from negative to positive, with two different isoprene schemes. However, as shown in Fig. 5 the influence of the isoprene scheme on free tropospheric O_3 is small relative to that from NO_x so that we do not expect errors in the isoprene scheme to significantly alter our conclusions. These results are consistent with Mao et al. (2013) as they show that a change in sign in the sensitivity of ozone to isoprene only affected their surface ozone concentrations by 2 ppb or less and therefore had an even smaller effect on free tropospheric ozone concentrations.

The contributions to the free tropospheric ozone in the the China outflow region are shown in Fig. 6. The O_3 distribution is more sensitive to the anthropogenic NO_x emissions from the coast rather than from the inland continent. The sensitivity hot spots clearly show a northeastward movement as the season progresses, from southeastern China (June) to Korea and Japan (August), reflecting the influence of the East Asian monsoon.

To understand the seasonal variation of O_3 production efficiency, we calculated the global-scale sensitivities of anthropogenic and lightning NO_x during December 2005–November 2006 with $4° \times 5°$ resolution. The values of sensitivities, as shown in Fig. 7, are significantly larger than those in Figs. 5 and 6, due to the change of grid size and smaller effect from initial condition. The sensitivity of O_3 to anthropogenic NO_x has a marked seasonal variation, increasing in the Northern Hemisphere from winter to the summer. Kondo et al. (2008) found the slope of eastern Asia O_3 formation to NO_x is proportional to HO_2 and thus increases from winter to spring. Increased solar radiation is another reason for the high O_3 production rate in the summer. Figure 7 also highlights the effect of anthropogenic NO_x from southwestern China, showing a significant effect on free troposphere O_3 over eastern China, particularly in September–November. Similar to anthropogenic NO_x, the contribution of lightning NO_x is maximum in the Northern Hemisphere summer, partly associated with the East Asian monsoon. The sensitivities of O_3 over eastern China and the China outflow region have similar distributions, although the China outflow O_3 is more sensitive to coastal emissions.

Table 2 shows the regional, total contributions of anthropogenic and lightning NO_x, calculated by summing the sensitivities shown in Fig. 7. Assuming an unchanged chemical environment, it can be explained as the percentage change of regional mean O_3 due to a 100 % change in NO_x emissions. For example, a 100 % increase of Chinese anthropogenic NO_x emissions in June–August 2006 will result in 10.2 % increase of tropospheric mean O_3 over eastern China. Of course, the result of an actual 100 % change of NO_x will be different because of nonlinear chemistry. Furthermore, this sensitivity depends on the modeled transport and the robustness of the chemical production of ozone. For example, if the production of ozone is too "fast" then the sensitivity of free tropospheric ozone to surface emissions is too small as too much ozone is produced in the boundary layer (where loss-mechanisms dominate) versus the free troposphere. To evaluate the sensitivities further, we enhanced Chinese anthropogenic NO_x emissions by 10 % uniformly as a perturbation. Using the initial conditions provided from the standard simulation, the 3-month perturbation simulations are started on 1 December 2005, 1 March 2006, 1 June 2006 and 1 September 2006, individually. The relative difference of regional mean O_3 between the perturbation and standard simulations is then multiplied by 10. As shown in Table 2, the results of the two methods are highly consistent, which demonstrates our sensitivity analysis works well. Similar to Wild et al. (2012), the consistency also confirms that 10 % NO_x perturbation gives a linear O_3 response over eastern Asia. Considering the high computation efficiency, adjoint sensitivity analysis is thus a good alternative to the traditional perturbation method.

As shown in Table 2, the effect of increased Chinese anthropogenic NO_x on free tropospheric O_3 is limited. Assuming an unchanged chemical environment, a 100 % increase of Chinese anthropogenic NO_x, during a 3-month period, will only result in a 2.4 % increase of free tropospheric O_3 in the winter and 10.2 % in the summer, associated with the chemical environment of China, which is is more inclined to be VOC limited. Because of the long O_3 lifetime in the free troposphere, O_3 from initial conditions has a substantial influence on the distribution of ozone. A 15-month continuous perturbation simulation, started on 1 September 2005, will enhance the effect of Chinese anthropogenic NO_x to 3.0 % in winter and 10.5 % in summer.

Because of the rapid growth of pollutant emissions, the transpacific transport of Asian pollutants to North America has attracted significant attention (Zhang et al., 2008; L. Zhang et al., 2009; Walker et al., 2010; Bertram et al., 2013; Lin et al., 2008, 2014a). The major transport mechanisms include the northeastward export of Asian pollution to about 50° N, and then the transport across the Pacific in midlatitude westerly winds (Liang et al., 2004, 2005). Over eastern China, the effect of anthropogenic NO_x emissions from the rest of Asia (ROA) on free tropospheric O_3 is that
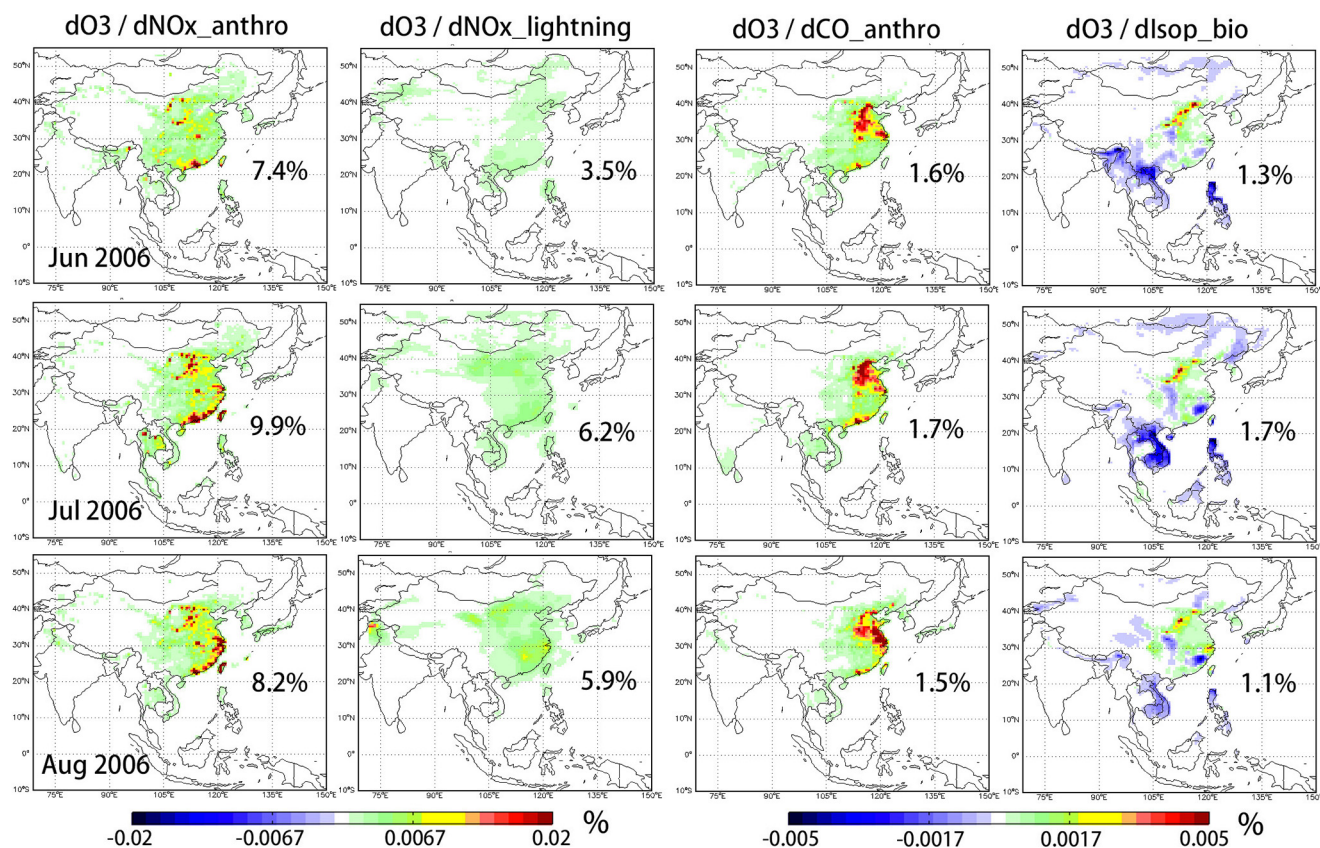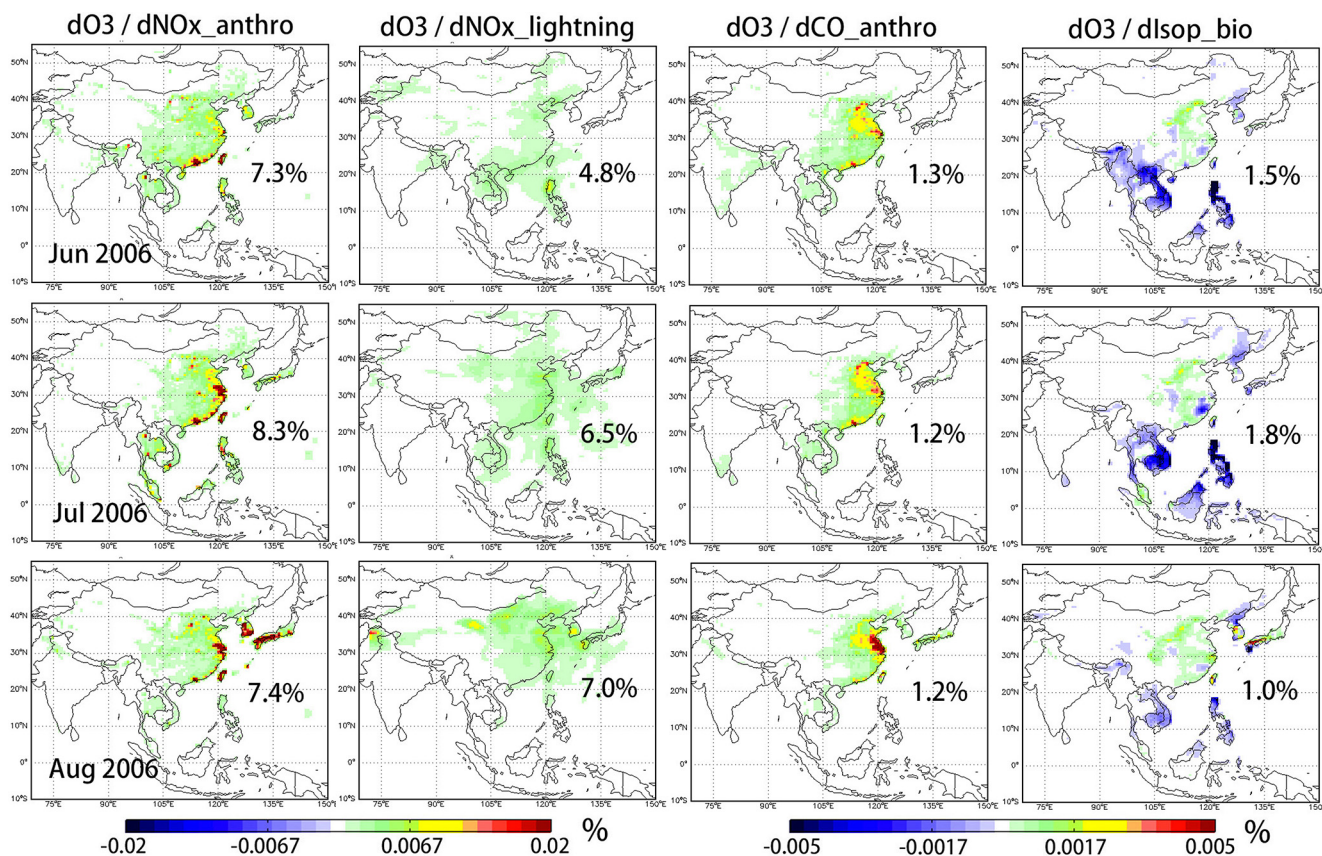
Figure 5. Contributions of anthropogenic NO_x, lightning NO_x, anthropogenic CO, biogenic isoprene on free tropospheric (819–396 hPa) O_3 over eastern China derived from the adjoint of GEOS-Chem in June, July and August 2006. The contributions can be explained as the percentage of change of regional mean ozone due to a fractional change in the emissions in a particular grid assuming an unchanged chemical environment. The numbers are the total of the absolute value of precursor contributions for the whole domain shown in the figures.

Table 2. Regional, total contributions of anthropogenic and lightning NO_x on free tropospheric (819–396 hPa) O_3 over eastern China and the China outflow region. The value can be explained as the percentage change of regional mean O_3 (eastern China, China outflow) due to 100 % increase of NO_x in a particular region (China and ROA). The regions of China and the ROA are defined in Fig. 3. The perturbation values (Pt) are the relative difference between standard and perturbation simulations.

Type		Eastern China				China outflow			
		DJF	MAM	JJA	SON	DJF	MAM	JJA	SON
NO_x anthro	China	2,4 %	5,2 %	10,2 %	7,0 %	2,6 %	5,5 %	8,6 %	5,8 %
	China (Pt)	2,6 %	5,3 %	10,2 %	6,8 %	2,9 %	5,8 %	8,5 %	5,7 %
	ROA	1,7 %	2,0 %	2,2 %	2,0 %	2,2 %	2,4 %	3,4 %	2,9 %
NO_x lightning	China	0,2 %	1,6 %	6,1 %	1,4 %	0,3 %	2,3 %	6,3 %	1,7 %
	ROA	0,8 %	2,2 %	2,6 %	1,9 %	1,2 %	3,1 %	3,9 %	2,8 %

of about 50 % of the Chinese local emissions in winter and spring, whereas the Chinese local emissions dominate in the summer and fall. Our results show that the influence of the ROA on O_3 pollution export is significant because the influence of the ROA is comparable with Chinese emissions in winter and about 50 % of the Chinese emissions in other seasons for the outflow region. The contribution of lightning NO_x over China is generally small relative to anthropogenic

emissions except during the summer (Table 2). The effect of the ROA lightning NO_x is similar to the Chinese contribution but slightly larger.

Figure 6. Contributions of anthropogenic NO_x, lightning NO_x, anthropogenic CO, and biogenic isoprene on free tropospheric (819–396 hPa) O_3 over China outflow region derived from the adjoint of GEOS-Chem in June, July and August 2006.

5   Summary

We quantified Asian O_3 and the contributions of its precursors, during the period December 2005–November 2006, using the GEOS-Chem model and O_3 precursor observations of NO_2 from OMI and CO from MOPITT. The 2006 global CO emissions are constrained with a 4-DVAR method, using MOPITT CO (version 6) measurements. In June 2006, the inversion increases the China anthropogenic CO emission by 11 %. The 2006 China NO_x emission is constrained with a regression-based multistep approach, using OMI data. In June 2006, the anthropogenic NO_x emission in China increased by 14 %.

The model simulation is evaluated with TES O_3 and CO observations. The modeled concentrations are underestimated for both O_3 and CO, but reproduce the O_3(CO) interannual variation. As with previous studies (Zhang et al., 2006; Voulgarakis et al., 2011; Kim et al., 2013), the modeled O_3–CO correlation and slope are consistent with the data. The updated inventories significantly reduce the bias relative to TES CO measurements, but the improvement on the O_3 simulation is not large ($\sim$ 1–2 %). The good agreement between model O_3 and CO and its correlations with obser-

vations from TES demonstrates the reliability of the model simulation, the chemical scheme and the updated CO inventories.

We quantified source contributions (NO_x, CO, VOC) to free tropospheric O_3 pollution over eastern China and the China outflow region with a sensitivity calculation approach. Our results show anthropogenic emissions from China are the major contributor to free tropospheric O_3 over eastern Asia and the corresponding outflow region. The anthropogenic emissions from the ROA have an important influence on free tropospheric O_3 over this region. The observed seasonal variation in O_3 is due to the seasonal change in the O_3 production efficiency, related to HO_2 and solar radiation. The contributions of lightning NO_x to free tropospheric O_3 from China and the ROA are small, except in June–August due to the effect of the East Asian monsoon. Finally, our result shows that China is the major contributor of anthropogenic VOCs, whereas the influence of biogenic VOCs is mainly from southeastern Asia.
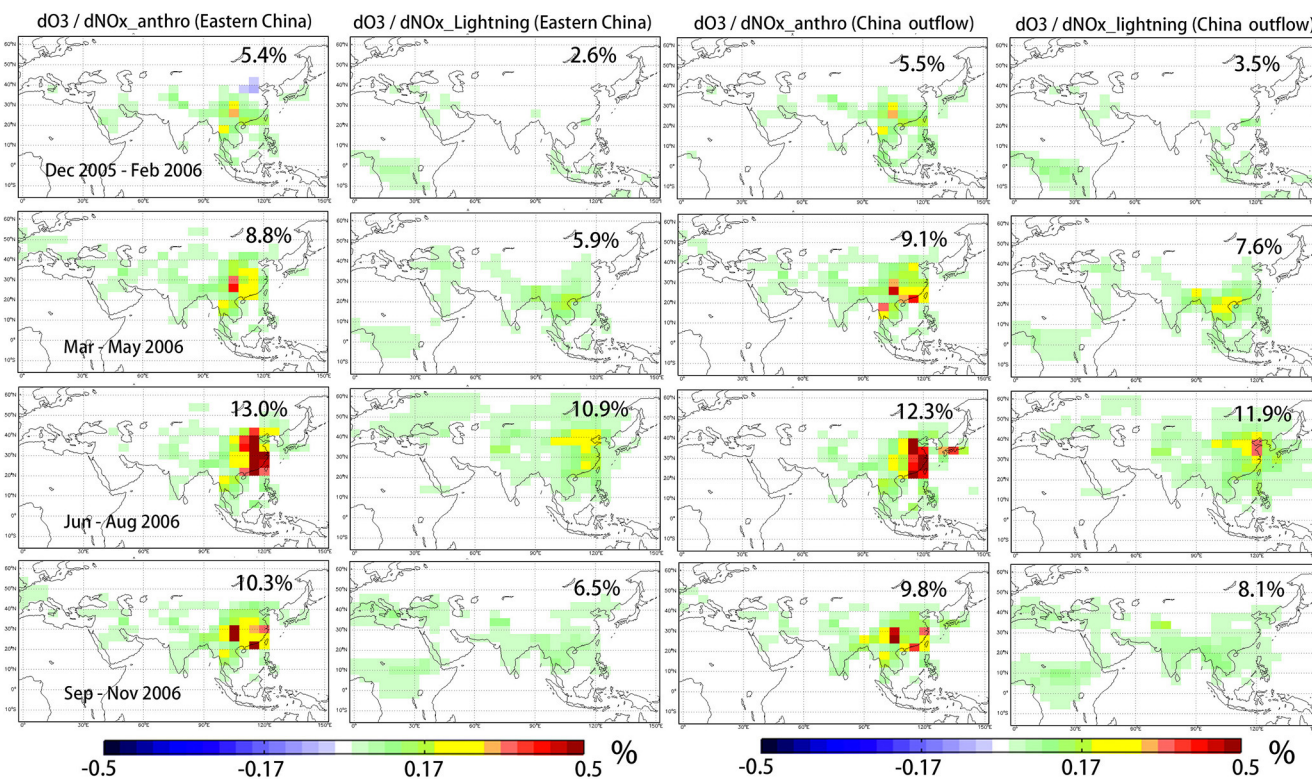
Figure 7. Contributions of anthropogenic NO_x and lightning NO_x on free tropospheric (819–396 hPa) O_3 over eastern China and the China outflow region in December 2005–November 2006.

The Supplement related to this article is available online at doi:10.5194/acp-15-99-2015-supplement.

References

Beer, R., Glavich, T. A., and Rider, D. M.: Tropospheric emission spectrometer for the Earth Observing System's Aura satellite, Appl. Optics, 40, 2356–2367, 2001.

Bertram, T. H., Perring, A. E., Wooldridge, P. J., Dibb, J., Avery, M. A., and Cohen, R. C.: On the export of reactive nitrogen from Asia: NO_x partitioning and effects on ozone, Atmos. Chem. Phys., 13, 4617–4630, doi:10.5194/acp-13-4617-2013, 2013.

Boersma, K. F., Eskes, H. J., Dirksen, R. J., van der A, R. J., Veefkind, J. P., Stammes, P., Huijnen, V., Kleipool, Q. L., Sneep, M., Claas, J., Leitão, J., Richter, A., Zhou, Y., and Brunner, D.: An improved tropospheric NO_2 column retrieval algorithm for the Ozone Monitoring Instrument, Atmos. Meas. Tech., 4, 1905–1928, doi:10.5194/amt-4-1905-2011, 2011.

Bowman, K. and Henze, D. K.: Attribution of direct ozone radiative forcing to spatially resolved emissions, Geophys. Res. Lett., 39, L22704, doi:10.1029/2012GL053274, 2012.

Brown-Steiner, B. and Hess, P.: Asian influence on surface ozone in the United States: a comparison of chemistry, seasonality, and transport mechanisms, J. Geophys. Res., 116, D17309, doi:10.1029/2011JD015846, 2011.

Chen, D., Wang, Y., McElroy, M. B., He, K., Yantosca, R. M., and Le Sager, P.: Regional CO pollution and export in China simulated by the high-resolution nested-grid GEOS-Chem model, Atmos. Chem. Phys., 9, 3825–3839, doi:10.5194/acp-9-3825-2009, 2009.

Deeter, M. N., Martìnez-Alonso, S., Edwards, D. P., Emmons, L. K., Gille, J. C., Worden, H. M., Pittman, J. V., Daube, B. C., and Wofsy, S. C.: Validation of MOPITT Version 5 thermal- infrared, near-infrared, and multispectral carbon monoxide profile retrievals for 2000–2011, J. Geophys. Res.-Atmos., 118, 6710–6725, 2013.

Duncan, B. N., Logan, J. A. Bey, I., Megretskaia, I. A., Yantosca, R. M., Novelli, P. C., Jones, N. B., and Rinsland, C. P.: Global budget of CO, 1988–1997: Source estimates and val-

idation with a global model, J. Geophys. Res., 112, D22301, doi:10.1029/2007JD008459, 2007.

Fortems-Cheiney, A., Chevallier, F., Pison, I., Bousquet, P., Szopa, S., Deeter, M. N., and Clerbaux, C.: Ten years of CO emissions as seen from Measurements of Pollution in the Troposphere (MOPITT), J. Geophys. Res., 116, D05304, doi:10.1029/2010JD014416, 2011.

Fu, T.-M., Jacob, D. J., Palmer, P. I., Chance, K., Wang, Y. X., Barletta, B., Blake, D. R., Stanton, J. C., and Pilling, M. J.: Space-based formaldehyde measurements as constraints on volatile organic compound emissions in east and south Asia and implications for ozone, J. Geophys. Res., 112, D06312, doi:10.1029/2006JD007853, 2007.

Gonzi, S., Feng, L., and Palmer, P. I.: Seasonal cycle of emissions of CO inferred from MOPITT profiles of CO: sensitivity to pyroconvection and profile retrieval assumptions, Geophys. Res. Lett., 38, L08813, doi:10.1029/2011GL046789, 2011.

Henze, D. K., Hakami, A., and Seinfeld, J. H.: Development of the adjoint of GEOS-Chem, Atmos. Chem. Phys., 7, 2413–2433, doi:10.5194/acp-7-2413-2007, 2007.

Jiang, Z., Jones, D. B. A., Worden, H. M., Deeter, M. N., Henze, D. K., Worden, J., Bowman, K. W., Brenninkmeijer, C. A. M., and Schuck, T. J.: Impact of model errors in convective transport on CO source estimates inferred from MOPITT CO retrievals, J. Geophys. Res.-Atmos., 118, 2073–2083, 2013.

Jiang, Z., Jones, D. B. A., Worden, J., Worden, H., Henze, D., and Wang, Y. X.: Regional data assimilation of multi-spectral MOPITT observations of CO over North America, in preparation, 2014a.

Jiang, Z., Jones, D. B. A., Worden, H. M., and Henze, D. K.: Sensitivity of inferred regional CO source estimates to the vertical structure in CO as observed by MOPITT, Atmos. Chem. Phys. Discuss., 14, 22939–22984, doi:10.5194/acpd-14-22939-2014, 2014b.

Kim, P. S., Jacob, D. J., Liu, X., Warner, J. X., Yang, K., Chance, K., Thouret, V., and Nedelec, P.: Global ozone-CO correlations from OMI and AIRS: constraints on tropospheric ozone sources, Atmos. Chem. Phys., 13, 9321–9335, doi:10.5194/acp-13-9321-2013, 2013.

Kondo, J., Hudman, R. C., Nakamura, K., Koike, M., Chen, G., Miyazaki, Y., Takegawa, N., Blake, D. R., Simpson, I. J., Ko, M., Kita, K., and Shirai, T.: Mechanisms that influence the formation of high-ozone regions in the boundary layer downwind of the Asian continent in winter and spring, J. Geophys. Res., 113, D15304, doi:10.1029/2007JD008978, 2008.

Kopacz, M., Jacob, D. J., Fisher, J. A., Logan, J. A., Zhang, L., Megretskaia, I. A., Yantosca, R. M., Singh, K., Henze, D. K., Burrows, J. P., Buchwitz, M., Khlystova, I., McMillan, W. W., Gille, J. C., Edwards, D. P., Eldering, A., Thouret, V., and Nedelec, P.: Global estimates of CO sources with high resolution by adjoint inversion of multiple satellite datasets (MOPITT, AIRS, SCIAMACHY, TES), Atmos. Chem. Phys., 10, 855–876, doi:10.5194/acp-10-855-2010, 2010.

Kuhns, H., Green, M., and Etyemezian, V.: Big Bend Regional Aerosol and Visibility Observational (BRAVO) Study Emissions Inventory, Report prepared for BRAVO Steering Committee, Desert Research Institute, Las Vegas, Nevada, 2003.

Lamsal, L. N., Martin, R. V., Padmanabhan, A., van Donkelaar, A., Zhang, Q., Sioris, C. E., Chance, K., Kurosu,

T. P., and Newchurch, M. J.: Application of satellite observations for timely updates to global anthropogenic NO_x emission inventories, Geophys. Res. Lett., 38, L05810, doi:10.1029/2010GL046476, 2011.

Lapina, K., Henze, D. K., Milford, J. B., Huang, M., Lin, M., Fiore, A. M., Carmichael, G., Pfister, G. G., and Bowman, K.: Assessment of source contributions to seasonal vegetative exposure to ozone in the U.S., J. Geophys. Res.-Atmos., 119, 324–340, 2014.

Levelt, P. F., van den Oord, G. H. J., Dobber, M. R., Malkki, A., Visser, H., de Vries, J., Stammes, P., Lundell, J. O. V., and Saari, H.: The Ozone Monitoring Instrument, IEEE T. Geosci. Remote, 44, 1093–1101, 2006.

Liang, Q., Jaegle, L., Jaffe, D. A., Weiss-Penzias, P., Heckman, A., and Snow, J. A.: Long- range transport of Asian pollution to the northeast Pacific: seasonal variations and transport pathways of carbon monoxide, J. Geophys. Res., 109, D23S07, doi:10.1029/2003JD004402, 2004.

Liang, Q., Jaegle, L., and Wallace, J. M.: Meteorological indices for Asian outflow and transpacific transport on daily to interannual timescales, J. Geophys. Res., 110, D18308, doi:10.1029/2005JD005788, 2005.

Lin, J.-T.: Satellite constraint for emissions of nitrogen oxides from anthropogenic, lightning and soil sources over East China on a high-resolution grid, Atmos. Chem. Phys., 12, 2881–2898, doi:10.5194/acp-12-2881-2012, 2012.

Lin, J.-T. and McElroy, M. B.: Detection from space of a reduction in anthropogenic emissions of nitrogen oxides during the Chinese economic downturn, Atmos. Chem. Phys., 11, 8171–8188, doi:10.5194/acp-11-8171-2011, 2011.

Lin, J.-T., Wuebbles, D. J., and Liang, X. Z.: Effects of intercontinental transport on surface ozone over the United States: present and future assessment with a global model, Geophys. Res. Lett., 35, L02805, doi:10.1029/2007GL031415, 2008.

Lin, J.-T., Liu, Z., Zhang, Q., Liu, H., Mao, J., and Zhuang, G.: Modeling uncertainties for tropospheric nitrogen dioxide columns affecting satellite-based inverse modeling of nitrogen oxides emissions, Atmos. Chem. Phys., 12, 12255–12275, doi:10.5194/acp-12-12255-2012, 2012.

Lin, J.-T., Pan, D., Davis, S. J., Zhang, Q., He, K., Wang, C., Streets, D. G., Wuebbles, D. J., and Guan, D.: China's international trade and air pollution in the United States, P. Natl. Acad. Sci. USA, 11, 1736–1741, doi:10.1073/pnas.1312860111, 2014a.

Lin, J.-T., Martin, R. V., Boersma, K. F., Sneep, M., Stammes, P., Spurr, R., Wang, P., Van Roozendael, M., Clémer, K., and Irie, H.: Retrieving tropospheric nitrogen dioxide from the Ozone Monitoring Instrument: effects of aerosols, surface reflectance anisotropy, and vertical profile of nitrogen dioxide, Atmos. Chem. Phys., 14, 1441–1461, doi:10.5194/acp-14-1441-2014, 2014b.

Liu, J. and Mauzerall, D. L.: Estimating the average time for intercontinental transport of air pollutants, Geophys. Res. Lett., 32, L11814, doi:10.1029/2005GL022619, 2005.

Luo, M., Rinsland, C., Fisher, B., Sachse, G., Diskin, G., Logan, J., Worden, H., Kulawik, S., Osterman, G., Eldering, A., Herman, R., and Shephard, M.: TES carbon monoxide validation with DACOM aircraft measurements during INTEX-B 2006, J. Geophys. Res., 112, D24S48, doi:10.1029/2007JD008803, 2007.

Mao, J., Paulot, F., Jacob, D. J., Cohen, R. C., Crounse, J. D., Wennberg, P. O., Keller, C. A., Hudman, R. C., Barkley, M. P.,

and Horowitz, L. W.: Ozone and organic nitrates over the eastern United States: sensitivity to isoprene chemistry, J. Geophys. Res.-Atmos., 118, 11256–11268, doi:10.1002/jgrd.50817, 2013.

Mao, Y. H., Li, Q. B., Henze, D. K., Jiang, Z., Jones, D. B. A., Kopacz, M., He, C., Qi, L., Gao, M., Hao, W.-M., and Liou, K.-N.: Variational estimates of black carbon emissions in the western United States, Atmos. Chem. Phys. Discuss., 14, 21865–21916, doi:10.5194/acpd-14-21865-2014, 2014.

Martin, R. V., Fiore, A. M., and Donkelaar, A. Van: Space-based diagnosis of surface ozone sensitivity to anthropogenic emissions, Geophys. Res. Lett., 31, L06120, doi:10.1029/2004GL019416, 2004.

Mijling, B., van der A, R. J., and Zhang, Q.: Regional nitrogen oxides emission trends in East Asia observed from space, Atmos. Chem. Phys., 13, 12003–12012, doi:10.5194/acp-13-12003-2013, 2013.

Millet, D. B., Jacob, D. J., Boersma, K. F., Fu, T. M., Kurosu, T. P., Chance, K., Heald, C. L., and Guenther, A.: Spatial distribution of isoprene emissions from North America derived from formaldehyde column measurements by the OMI satellite sensor, J. Geophys. Res., 113, D02307, doi:10.1029/2007JD008950, 2008.

Naik, V., Voulgarakis, A., Fiore, A. M., Horowitz, L. W., Lamarque, J.-F., Lin, M., Prather, M. J., Young, P. J., Bergmann, D., Cameron-Smith, P. J., Cionni, I., Collins, W. J., Dalsøren, S. B., Doherty, R., Eyring, V., Faluvegi, G., Folberth, G. A., Josse, B., Lee, Y. H., MacKenzie, I. A., Nagashima, T., van Noije, T. P. C., Plummer, D. A., Righi, M., Rumbold, S. T., Skeie, R., Shindell, D. T., Stevenson, D. S., Strode, S., Sudo, K., Szopa, S., and Zeng, G.: Preindustrial to present-day changes in tropospheric hydroxyl radical and methane lifetime from the Atmospheric Chemistry and Climate Model Intercomparison Project (ACCMIP), Atmos. Chem. Phys., 13, 5277-5298, doi:10.5194/acp-13-5277-2013, 2013.

Olivier, J. G. J. and Berdowski, J. J. M.: Global emissions sources and sinks, in: The Climate System, edited by: Berdowski, J., Guicherit, R., and Heij, B. J., 33–78, A. A. Balkema Publishers/Swets & Zeitlinger Publishers, Lisse, the Netherlands, 2001.

Parrington, M., Jones, D. B. A., Bowman, K. W., Horowitz, L. W., Thompson, A. M., Tarasick, D. W., and Witte, J. C.: Estimating the summertime tropospheric ozone distribution over North America through assimilation of observations from the Tropospheric Emission Spectrometer, J. Geophys. Res., 113, D18307, doi:10.1029/2007JD009341, 2008.

Parrington, M., Palmer, P. I., Henze, D. K., Tarasick, D. W., Hyer, E. J., Owen, R. C., Helmig, D., Clerbaux, C., Bowman, K. W., Deeter, M. N., Barratt, E. M., Coheur, P.-F., Hurtmans, D., Jiang, Z., George, M., and Worden, J. R.: The influence of boreal biomass burning emissions on the distribution of tropospheric ozone over North America and the North Atlantic during 2010, Atmos. Chem. Phys., 12, 2077–2098, doi:10.5194/acp-12-2077-2012, 2012.

Pechony, O., Shindell, D. T., and Faluvegi, G.: Direct top-down estimates of biomass burning CO emissions using TES and MOPITT versus bottom-up GFED inventory, J. Geophys. Res.-Atmos., 118, 8054–8066, doi:10.1002/jgrd.50624, 2013.

Shim, C., Wang, Y., Choi, Y., Palmer, P. I., Abbot, D. S., and Chance, K.: Constraining global isoprene emissions with Global Ozone Monitoring Experiment (GOME) formalde-

hyde column measurements, J. Geophys. Res., 110, D24301, doi:10.1029/2004JD005629, 2005.

Shindell, D. T., Faluvegi, G., Stevenson, D. S., Krol, M. C., Emmons, L. K., Lamarque, J. F., Pétron, G., Dentener, F. J., Ellingsen, K., Schultz, M. G., Wild, O., Amann, M., Atherton, C. S., Bergmann, D. J., Bey, I., Butler, T., Cofala, J., Collins, W. J., Derwent, R. G., Doherty, R. M., Drevet, J., Eskes, H. J., Fiore, A. M., Gauss, M., Hauglustaine, D. A., Horowitz, L. W., Isaksen, I. S. A., Lawrence, M. G., Montanaro, V., Müller, J. F., Pitari, G., Prather, M. J., Pyle, J. A., Rast, S., Rodriguez, J. M., Sanderson, M. G., Savage, N. H., Strahan, S. E., Sudo, K., Szopa, S., Unger, N., van Noije, T. P. C., and Zeng, G.: Multimodel simulations of carbon monoxide: Comparison with observations and projected near-future changes, J. Geophys. Res., 111, D19306, 10.1029/2006JD007100 2006.

Singh, K., Jardak, M., Sandu, A., Bowman, K., Lee, M., and Jones, D.: Construction of non-diagonal background error covariance matrices for global chemical data assimilation, Geosci. Model Dev., 4, 299–316, doi:10.5194/gmd-4-299-2011, 2011.

Valin, L. C., Russell, A. R., Hudman, R. C., and Cohen, R. C.: Effects of model resolution on the interpretation of satellite NO_2 observations, Atmos. Chem. Phys., 11, 11647–11655, doi:10.5194/acp-11-11647-2011, 2011.

van der Werf, G. R., Randerson, J. T., Giglio, L., Collatz, G. J., Mu, M., Kasibhatla, P. S., Morton, D. C., DeFries, R. S., Jin, Y., and van Leeuwen, T. T.: Global fire emissions and the contribution of deforestation, savanna, forest, agricultural, and peat fires (1997–2009), Atmos. Chem. Phys., 10, 11707–11735, doi:10.5194/acp-10-11707-2010, 2010.

Verstraeten, W. W., Boersma, K. F., Zörner, J., Allaart, M. A. F., Bowman, K. W., and Worden, J. R.: Validation of six years of TES tropospheric ozone retrievals with ozonesonde measurements: implications for spatial patterns and temporal stability in the bias, Atmos. Meas. Tech., 6, 1413–1423, doi:10.5194/amt-6-1413-2013, 2013.

Vestreng, V. and Klein, H.: Emission data reported to UNECE/EMEP, Quality assurance and trend analysis and Presentation of WebDab, Norwegian Meteorological Institute, Oslo, Norway, MSC-W Status Report, 2002.

Voulgarakis, A., Telford, P. J., Aghedo, A. M., Braesicke, P., Faluvegi, G., Abraham, N. L., Bowman, K. W., Pyle, J. A., and Shindell, D. T.: Global multi-year O_3-CO correlation patterns from models and TES satellite observations, Atmos. Chem. Phys., 11, 5819–5838, doi:10.5194/acp-11-5819-2011, 2011.

Walker, T. W., Martin, R. V., van Donkelaar, A., Leaitch, W. R., MacDonald, A. M., Anlauf, K. G., Cohen, R. C., Bertram, T. H., Huey, L. G., Avery, M. A., Weinheimer, A. J., Flocke, F. M., Tarasick, D. W., Thompson, A. M., Streets, D. G., and Liu, X.: Trans-Pacific transport of reactive nitrogen and ozone to Canada during spring, Atmos. Chem. Phys., 10, 8353–8372, doi:10.5194/acp-10-8353-2010, 2010.

Wang, Y. X., McElroy, M. B., Jacob, D. J., and Yantosca, R. M.: A nested grid formulation for chemical transport over Asia: applications to CO, J. Geophys. Res., 109, D22307, doi:10.1029/2004JD005237, 2004.

Wang, Y., Konopka, P., Liu, Y., Chen, H., Müller, R., Plöger, F., Riese, M., Cai, Z., and Lü, D.: Tropospheric ozone trend over Beijing from 2002–2010: ozonesonde measurements

and modeling analysis, Atmos. Chem. Phys., 12, 8389–8399, doi:10.5194/acp-12-8389-2012, 2012.

Wild, O., Fiore, A. M., Shindell, D. T., Doherty, R. M., Collins, W. J., Dentener, F. J., Schultz, M. G., Gong, S., MacKenzie, I. A., Zeng, G., Hess, P., Duncan, B. N., Bergmann, D. J., Szopa, S., Jonson, J. E., Keating, T. J., and Zuber, A.: Modelling future changes in surface ozone: a parameterized approach, Atmos. Chem. Phys., 12, 2037–2054, doi:10.5194/acp-12-2037-2012, 2012.

Worden, H. M., Logan, J. A., Worden, J. R., Beer, R., Bowman, K., Clough, S. A., Eldering, A., Fisher, B. M., Gunson, M. R., Herman, R. L., Kulawik, S. S., Lampel, M. C., Luo, M., Megretskaia, I. A., Osterman, G. B., and Shephard, M. W.: Comparisons of Tropospheric Emission Spectrometer (TES) ozone profiles to ozonesondes: methods and initial results, J. Geophys. Res., 112, D03309, doi:10.1029/2006JD007258, 2007.

Worden, H. M., Deeter, M. N., Edwards, D. P., Gille, J. C., Drummond, J. R., and Neìdeìlec, P.: Observations of near surface carbon monoxide from space using MOPITT multispectral retrievals, J. Geophys. Res., 115, D18314, doi:10.1029/2010JD014242, 2010.

Worden, J., Wecht, K., Frankenberg, C., Alvarado, M., Bowman, K., Kort, E., Kulawik, S., Lee, M., Payne, V., and Worden, H.: CH_4 and CO distributions over tropical fires during October 2006 as observed by the Aura TES satellite instrument and modeled by GEOS-Chem, Atmos. Chem. Phys., 13, 3679–3692, doi:10.5194/acp-13-3679-2013, 2013.

Yan, Y.-Y., Lin, J.-T., Kuang, Y., Yang, D., and Zhang, L.: Tropospheric carbon monoxide over the Pacific during HIPPO: two-way coupled simulation of GEOS-Chem and its multiple nested models, Atmos. Chem. Phys. Discuss., 14, 18961–18996, doi:10.5194/acpd-14-18961-2014, 2014.

Yang, Y., Liao, H., and Li, J.: Impacts of the East Asian summer monsoon on interannual variations of summertime surface-layer ozone concentrations over China, Atmos. Chem. Phys., 14, 6867–6879, doi:10.5194/acp-14-6867-2014, 2014.

Zhang, L., Jacob, D. J., Bowman, K. W., Logan, J. A., Turquety, S., Hudman, R. C., Li, Q.- B., Beer, R., Worden, H. M., Worden, J. R., Rinsland, C. P., Kulawik, S. S., Lampel, M. C., Shephard, M. W., Fisher, B. M., Eldering, A., and Avery, M. A.: Ozone-CO correlations determined by the TES satellite instrument in continental outflow regions, Geophys. Res. Lett., 33, L18804, doi:10.1029/2006GL026399, 2006.

Zhang, L., Jacob, D. J., Boersma, K. F., Jaffe, D. A., Olson, J. R., Bowman, K. W., Worden, J. R., Thompson, A. M., Avery, M. A., Cohen, R. C., Dibb, J. E., Flock, F. M., Fuelberg, H. E., Huey, L. G., McMillan, W. W., Singh, H. B., and Weinheimer, A. J.: Transpacific transport of ozone pollution and the effect of recent Asian emission increases on air quality in North America: an integrated analysis using satellite, aircraft, ozonesonde, and surface observations, Atmos. Chem. Phys., 8, 6117–6136, doi:10.5194/acp-8-6117-2008, 2008.

Zhang, L., Jacob, D. J., Kopacz, M., Henze, D. K., Singh, K., and Jaffe, D. A.: Intercontinental source attribution of ozone pollution at western U.S. sites using an adjoint method, Geophys. Res. Lett., 36, L11810, doi:10.1029/2009GL037950, 2009.

Zhang, Q., Streets, D. G., Carmichael, G. R., He, K. B., Huo, H., Kannari, A., Klimont, Z., Park, I. S., Reddy, S., Fu, J. S., Chen, D., Duan, L., Lei, Y., Wang, L. T., and Yao, Z. L.: Asian emissions in 2006 for the NASA INTEX-B mission, Atmos. Chem. Phys., 9, 5131–5153, doi:10.5194/acp-9-5131-2009, 2009.

Zhang, Q., Yuan, B., Shao, M., Wang, X., Lu, S., Lu, K., Wang, M., Chen, L., Chang, C.-C., and Liu, S. C.: Variations of ground-level O_3 and its precursors in Beijing in summertime between 2005 and 2011, Atmos. Chem. Phys., 14, 6089–6101, doi:10.5194/acp-14-6089-2014, 2014.